Surface Science 65 (1977) 511–531

SURFACE ENERGY AND SOLUTE STRAIN ENERGY EFFECTS IN SURFACE SEGREGATION

P. WYNBLATT and R.C. KU
Research Staff, Ford Motor Company, Dearborn, Michigan 48121, USA

Received 22 October 1976; manuscript received in final form 22 February 1977

Previous models of surface segregation have generally been based on the assumption that a decrease in surface free energy constitutes the predominant driving force for the phenomenon. In contrast, grain boundary segregation models have been founded on the postulate that the major driving force for that phenomenon is the reduction in lattice strain energy which accompanies the transfer of misfitting solute atoms from the lattice to the boundary. These two concepts have been combined here into a single unified formalism of surface segregation. In addition, the temperature dependence of surface composition of both nickel-rich and gold-rich nickel-gold alloys has been measured by Auger electron spectroscopy. Comparisons of the predictions of the combined formalism with the experimental results show excellent agreement between measured and calculated heats of adsorption (segregation). Furthermore, the present formalism provides estimates of the entropies of adsorption which can be used to explain apparent incompatibilities between the behavior of gold-rich and nickel-rich alloys.

1. Introduction

The recent development and maturation of several surface analysis techniques has prompted renewed interest in the phenomenon of interfacial segregation. This phenomenon, which manifests itself as a difference in composition between an interface and the adjoining phases, plays an important role in such areas as mechanical behavior, kinetics of phase transformations and the catalytic properties of alloys.

A macroscopic thermodynamic formalism describing interfacial segregation has been available since the time of Gibbs [1], but more recently, a number of microscopic statistical (Ising type) models have evolved [2–9] which allow a simpler evaluation of experimental results. Over the past few years, the results of *surface* segregation measurements have almost invariably been interpreted by means of models in which a decrease in surface free energy is assumed to be the predominant driving force for the segregation process (for example, the model of Defay et al. [2]). In contrast, the interpretation of *grain-boundary* segregation experiments has generally been based on the assumption that a decrease in lattice strain energy, associated with misfitting solute atoms, provides the driving force for the process (as enunciated, for example, by McLean [3]). It is clear, however, that any complete

treatment of equilibrium interfacial composition must involve minimization of the total system free energy, which includes contributions from both interfacial free energy and the lattice solute energy strain of the alloy.

When considered separately, the surface free energy and solute strain energy effects can lead to qualitatively different predictions of the component which segregates to the surface of a dilute binary alloy. For example, in a hypothetical, ideal A–B solid solution in which the pure component A possesses a lower surface energy than pure component B, minimization of surface free energy would dictate a higher concentration of A in the surface than in the bulk of the alloy, for *all* bulk compositions of the alloy. In contrast, the solute strain energy concept would predict a higher concentration of the *solute* in the surface than in the bulk. Thus, the two effects would tend to reinforce one another in the case of a B-rich alloy whereas they would tend to counteract one another in an A-rich alloy.

The purpose of this paper is to test the relative importance of the two effects outlined above: (a) by determining experimentally the relationship between the surface and bulk compositions in dilute alloys having compositions at either extreme of a given binary system and (b) by comparing the experimental results with theoretical estimates of surface segregation, based on a model which combines both surface energy and solute strain energy effects.

The gold–nickel system was chosen as a suitable subject for this study, for a number of reasons. First, gold and nickel form a continuous set of solid solutions at higher temperatures, and thus the dilute alloys at both extremes of the equilibrium diagram possess the same structure. Second, this system has a strong tendency to cluster (indeed, the system shows a well-defined miscibility gap) and thus avoid certain experimental problems expected with alloys which display a tendency to order [8]. Third, the differences in the surface energies and atomic sizes of nickel and gold are appreciable and should therefore provide adequate driving force for both effects. Finally, previous studies of surface segregation in several Ni-rich Ni–Au alloys have shown that gold segregates strongly enough to present little experimental difficulty in the determination of precise surface compositions [10,11].

2. Experimental procedure and results

2.1. Sample preparation

Four different alloys, having nominal compositions of Ni–0.05 at% Au, Au–0.5 at% Ni, Au–2 at% Ni and Au–5 at% Ni, were made up for this study. The alloys were melted in high purity recrystallized alumina crucibles under an inert atmosphere. All alloys were then rolled down to 0.4 mm thick foils. Chemical analyses performed on samples of the foil are reported in table 1. The materials were polycrystalline with a grain size of the order of 100 μm.

In experiments on each of the four alloys studied, a rectangular piece of foil,

Table 1

Nominal composition	Chemical analysis
Ni – 0.05 at% Au	Ni – 0.054 at% Au
Au – 2 at% Ni	Au – 2.03 at% Ni
Au – 5 at% Ni	Au – 5.0 at% Ni

measuring about 4 X 10 mm, was mounted onto a 1.5 mm thick Ta plate sample holder, and a chromel–alumel thermocouple was spot welded to one corner. The specimen and holder were then inserted into an ultrahigh vacuum system equipped with an electron gun and cylindrical mirror analyzer for Auger electron spectroscopy (AES), an inert gas sputtering gun, and a quadruple mass spectrometer for residual gas analysis. The holder and sample were mounted on an electron gun which was used to heat the assembly by electron bombardment. In addition to the sample, pure gold and nickel foils were placed in the system to act as standards for surface analysis by AES. The base pressure in the vacuum system during these experiments was $\sim 2 \times 10^{-10}$ Torr.

After insertion into the system, a sample was first sputtered clean and then heated to the temperature range of interest, whereupon impurities invariably segregated to the surface, as evidenced by the appearance of sulfur Auger peaks in the case of nickel-rich alloys and of carbon peaks in the case of gold-rich alloys. The samples were cleaned of these impurities by repeated heating in oxygen at $\sim 10^{-7}$ Torr. followed by heating in hydrogen or by sputtering. This cleaning procedure was continued until the Auger spectrum showed only small amounts of the impurities (less than 0.05 monolayers sulfur and no detectable carbon), after holding at temperature for suitable times, which ranged from a few minutes to several hours, depending on the temperature of the experiment.

2.2. Measurement of surface segregation

A measure of surface composition was obtained in these experiments from the peak to peak height of the Au 70 eV and Ni 61 eV Auger transitions plotted in the derivative mode. These transitions were selected for their short mean escape depths and hence, high surface sensitivity. A mean escape depth of ~4 Å has been measured at ~70 eV for gold [12] and at ~90 eV for nickel [13]. Unless otherwise noted, the Auger spectra reported here were obtained using a primary beam energy of 2500 eV and a modulation amplitude of 5 V (peak to peak). Typical spectra obtained in the energy range of interest from the pure gold and nickel standards, as well as from two sputter-cleaned alloys, are shown in fig. 1.

After the cleaning treatment described in section 2.1, a sample was heated to a given temperature, held there for some time and then quenched to about 150°C at

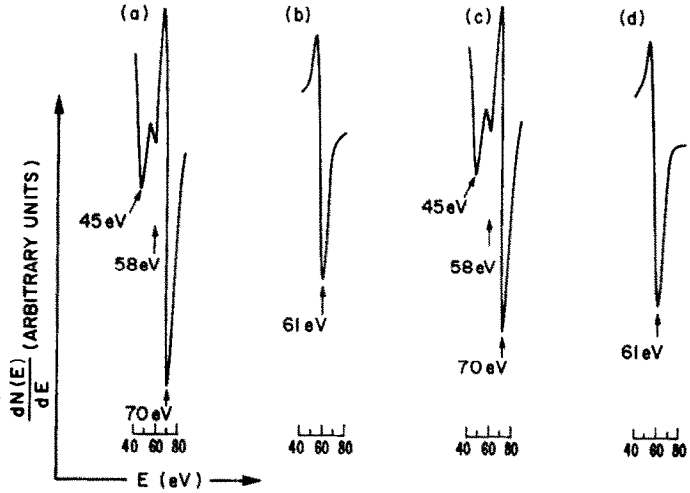

Fig. 1. Typical Auger spectra from (a) gold standard, (b) sputtered Ni–0.05 at% Au alloy, (c) sputtered Au–5 at% Ni alloy, (d) nickel standard.

a rate of ~300°C/min. At that point, an Auger spectrum was obtained from the sample. The sample was then heated back to the heat treatment temperature at a rate of ~600°C/min and the whole procedure repeated until no further change was observed in the Auger spectrum from the sample. Typical results from such an experiment, showing changes in the Au/Ni peak height ratios as a function of time, are shown in fig. 2.

Although it would have been preferable to obtain Auger spectra from the sample while it was being held at temperature, Auger traces taken from the sample while the heating system was operative were found to be too noisy for precision surface composition measurements. This noisiness (which manifested itself as shifts in peak energy and irreproducible peak to peak height) was probably due to penetration

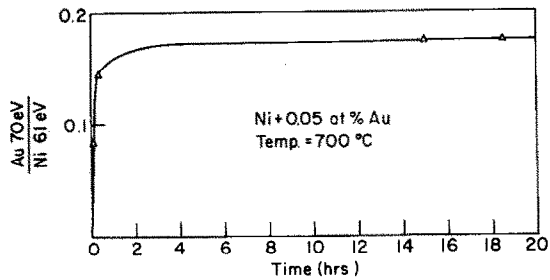

Fig. 2. Dependence of Au/Ni Auger peak ratio on holding time at temperature, illustrating rate of approach to equilibrium.

into the analyzer of stray electrons originating from the electron bombardment heater.

Measurements on quenched samples are subject to question when the kinetics of equilibration are so rapid, below the heat treatment temperature, that the surface composition undergoes changes during the quench. However, under those conditions, samples quenched from any temperature above some critical rapid equilibration temperature will all display the same surface composition, as has been shown by Burton et al. [11]. This type of behavior was not observed in the present experiments *. In addition, the noisy condition which prevented the gathering of useful spectra could be eliminated by switching the heating electron bombardment source off. Thus, limited Auger traces covering the important 50 to 80 eV range could be initiated immediately after turning the heater off, and could be obtained within a time span of ~6 sec, during which period the temperature drop from the heat treatment temperature was only ~30°C. Although not performed routinely (because of increased experimental scatter), this procedure invariably gave Au/Ni peak ratios that were within experimental error of traces taken after quenching. This type of experiment confirmed that the technique used here did indeed yield Auger spectra representative of the equilibrated alloy surface.

3. Results

3.1. Raw data

Representative Auger spectra obtained from equilibrated sample surface are presented in fig. 3. Results derived from such spectra, for the nickel rich alloy, are summarized in fig. 4 as a plot of Au/Ni Auger peak ratio versus equilibration temperature. The plot shows a strong temperature dependence of surface composition, indicating that substantial surface segretation of gold occurs in that alloy. The numbers in parenthesis associated with the points indicate the holding time (in hours) at the heat treatment temperature. These times are generally consistent with those estimated from solutions of the diffusion equation corresponding to segregation to a planar interface [3]. The procedure used to convert peak ratios into surface compositions is discussed in the following section.

The acquisition of the corresponding data from gold-rich alloys was somewhat more involved because of the complexity of the Auger spectrum of pure gold in the 45 to 70 eV region, and the rather weak segregation of nickel in those alloys. Auger spectra obtained from pure gold at a modulation amplitude of 1 V (for better resolution) showed peaks at 70, 66, 62, 58 and 45 eV, in reasonable agreement with

* This may indicate either that the quenching rates obtained by Burton et al. [11] were lower than reported, or that the cooling rate at the critical near-surface region, in the present experiments, was higher than actually measured.

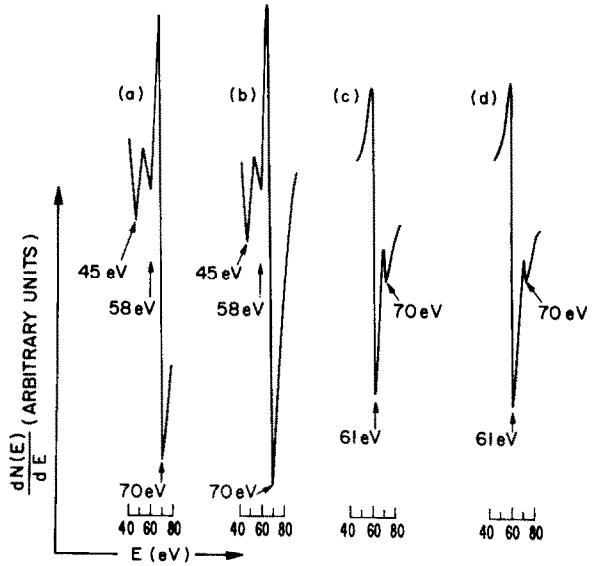

Fig. 3. Examples of Auger spectra taken from equilibrated alloy surfaces. (a) and (b) Au–5 at% Ni alloy equilibrated at 295 and 810°C respectively; (c) and (d) Ni–0.05 at% Au alloy equilibrated at 750 and 800°C respectively.

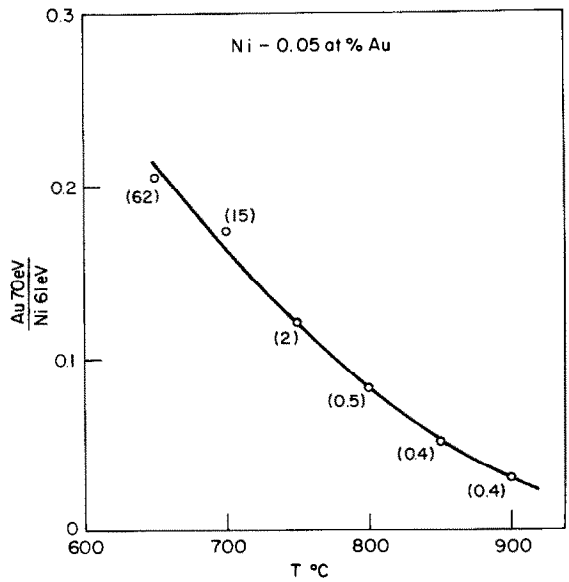

Fig. 4. Equilibrium values of the Au/Ni Auger peak ratio as a function of temperature for the Ni–0.05 at% Au alloy. Numbers in parentheses are equilibration times in hours.

the spectrum published in the Handbook of Auger Electron Spectroscopy [14]. The latter source shows labelled peaks at 69, 66, 56 and 43 eV as well as an unlabelled peak between 66 and 56 V which corresponds both in shape and relative magnitude to the peak we observed at 62 eV. The Ni 61 eV peak overlaps both the 62 and 58 eV gold peaks, and as a result, it tends to be washed out in the spectrum of alloys containing only small amounts of nickel. The gold spectrum obtained at our standard modulation amplitude of 5 V (see fig. 1a) displays only the 70, 58 and 45 eV peaks. In alloys containing small amounts of nickel (up to 5 at% in this case), and at a modulation amplitude of 5 V, the Ni 61 eV peak does not appear in the spectrum, but rather the relative peak-to-peak amplitude of the Au 58 eV peak increases with increasing nickel content without significant change in peak energy (see figs. 3a and 3b). Thus, results on Au-rich alloys are reported here as a ration of the magnitudes of the 58 eV transition (which contains contributions from both gold and nickel) to the Au 70 eV transition. The calibration of this ratio in terms of surface composition will also be discussed in section 3.2. The results obtained are shown in fig. 5. This figure shows some temperature dependence of surface composition for the 2 and 5 at% nickel alloys indicating definite, but weak, surface segregation of nickel. No evidence of surface segregation was found in the 0.5 at% Ni alloy, but the average value of the 58 eV to 70 eV peak ratio for that alloy, as well as the corresponding value of the ratio for pure gold, are also shown in fig. 5. The equilibration times,

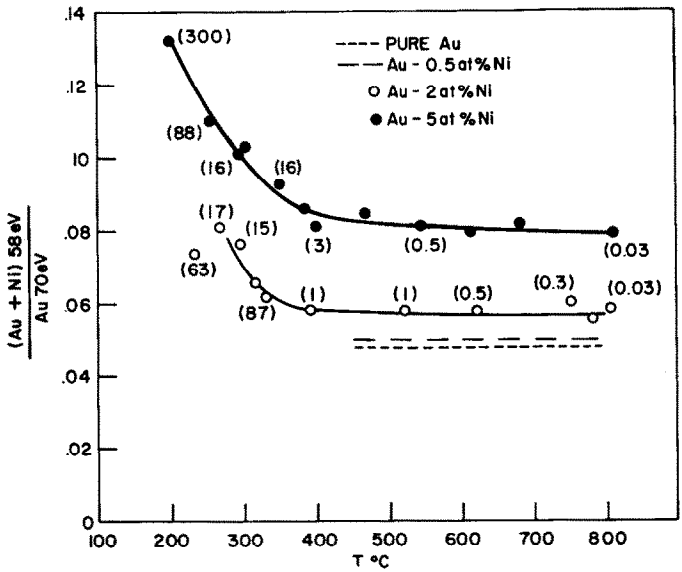

Fig. 5. Equilibrium values of the (Au + Ni) 58 eV/Ni 70 eV auger peak ratio for various gold-rich alloys (see text). Numbers in parentheses are equilibration times in hours.

shown in parenthesis, were also generally consistent with expected segregation kinetics [3].

3.2. Estimation of surface composition

A reliable method for the translation of Auger spectra into surface compositions is unavailable as yet. On the one hand, a number of studies on alloys of uniform composition have shown the existence of a reasonably linear relationship between the peak-to-peak amplitude of Auger transitions and the atomic fraction of the element producing the transition [15,16]. On the other hand, there is little doubt that segregated alloys represent a more complex case than uniform alloys, in view of the presence of concentration gradients near the surface. Thus, for example, back scattering effects would be expected to enhance somewhat the signal from nickel segregated at the surface of gold, in comparison with the signal from the same number of nickel atoms situated on a nickel substrate; whereas the opposite argument would apply in the case of gold segregated to a nickel surface. While excellent discussions of the proper formalism for inclusion of backscattering as well as other corrections in surface segregation measurements have already appeared [17,18], those corrections cannot reliably be applied at this time. Thus for our purposes here, we shall assume that a linear relationship between peak-to-peak amplitude and atomic fraction is obeyed, although it is recognized that this represents only a first order approximation. By using this approximation, it is possible to express the surface atomic fraction of element A in an alloy surface as:

$$X_A^s = P_{A\text{-}a}/P_{A\text{-}st}, \tag{1}$$

where $P_{A\text{-}a}$ and $P_{A\text{-}st}$ are the peak-to-peak amplitudes of the Auger signal from element A in the alloy and a pure A standard, respectively. For comparison of experiment with theory we require experimental values of the ratio, X_A^s/X_B^s, which can be obtained directly from eq. (1) as:

$$\frac{X_A^s}{X_B^s} = \frac{X_A^s}{1 - X_A^s} = \frac{P_{A\text{-}a}}{P_{A\text{-}st} - P_{A\text{-}a}}. \tag{2}$$

Alternatively, this ratio may be obtained from the Auger peaks of the two components in a binary alloy:

$$\frac{X_A^s}{X_B^s} = \frac{P_{A\text{-}a}}{P_{A\text{-}st}} \frac{P_{B\text{-}st}}{P_{B\text{-}a}}. \tag{3}$$

Both of these methods have been used to determine the surface composition of the nickel-rich alloys.

In the case of the gold-rich alloys, the situation is more complex as a result of overlap of the Ni 61 eV and Au 58 eV peaks, mentioned in section 3.1. As pointed

out earlier, it was found that small amounts of nickel contributed to an increase in the peak-to-peak amplitude of the Au 58 eV transition, without significant change in the peak energy. The following procedure was used to obtain a quantitative relationship between the magnitude of the 58 eV peak and the surface Ni/Au ratio. The detailed shapes of the Au 58 eV and Ni 61 eV peaks were obtained on an expanded scale from the pure gold and nickel standards respectively. Each peak shape was then fitted to a polynomial expression, and these expressions added for different Ni/Au atomic ratios, assuming as above a linear dependence of peak-to-peak amplitude on surface atomic fraction. The results of this computation are given in fig. 6, as a ratio of the computed peak-to-peak amplitude for the combined 58 eV and 61 eV transitions to the Au 70 eV transition, plotted against the atomic fraction ratio X^s_{Ni}/X^s_{Au}. Over the range of nickel compositions of interest, i.e. X^s_{Ni} = 0 to 0.2, the plot is almost linear, and the computed energy shift of the combined peak is about 1 eV. The curve of fig. 6 was used to convert experimental ratios of the 58 eV to 70 eV transitions into X^s_{Ni}/X^s_{Au}. A measure of the validity of this procedure is demonstrated by a comparison with some experimental points also plotted in that figure. The point corresponding to $X^s_{Ni}/X^s_{Au} = 0.005$ represents the average value of the experimental ratio obtained from the Au–0.5 at% Ni alloy, a composition for which no measurable segregation was observed, while the points for $X^s_{Ni}/X^s_{Au} = 0.02$ and 0.053 represent values of the ratio obtained from the other two gold-rich alloys at 800°C (c.f. fig. 5). As can be seen, the points corresponding to the two more dilute alloys fall quite close to the calibration curve. The point corresponding to the 5 at% Ni alloy falls somewhat above the curve implying some surface enrichment of nickel in that case, an implication which is consistent with the

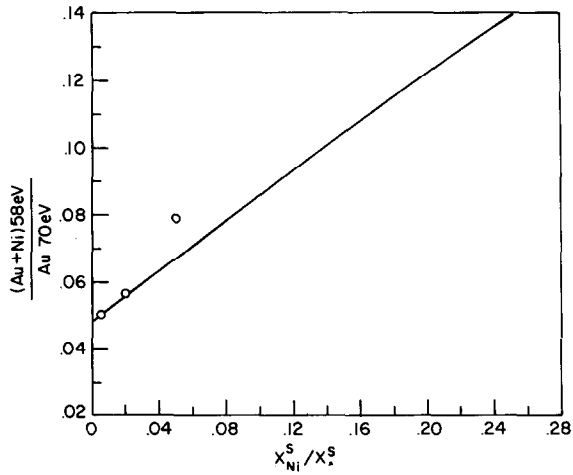

Fig. 6. Calibration curve for conversion of the experimental (Au + Ni) 58 eV/Au 70 eV Auger peak ratio into a surface atom fraction ratio, X^s_{Ni}/X^s_{Au} (see text).

Table 2

Ni–0.05 at% Au			Au–5 at% Ni		Au–2 at% Ni	
Temperature (°C)	X^s_{Au}/X^s_{Ni} by eq. (2)	X^s_{Au}/X^s_{Ni} by eq. (3)	Temperature (°C)	X^s_{Ni}/X^s_{Au} from fig. 6	Temperature (°C)	X^s_{Ni}/X^s_{Au} from fig. 6
650	0.143	0.146	200	0.230	232	0.067
700	0.112	0.124	255	0.166	268	0.087
750	0.081	0.086	295	0.141	295	0.074
800	0.054	0.059	302	0.146	315	0.046
850	0.034	0.037	350	0.119	330	0.035
900	0.018	0.021	384	0.100	390	0.027
			400	0.087	520	0.025
			467	0.097	620	0.025
			546	0.087	750	0.032
			612	0.083	780	0.020
			680	0.089	805	0.026
			810	0.082		

existence of a finite temperature dependence at 800°C in the appropriate curve of fig. 5. This general consistency between the calculated calibration curve and the corresponding experimental results enhances our confidence in the procedure used here to relate Auger spectra to surface composition.

The surface compositions obtained by these procedures for all three alloys, are listed in table 2. For the case of the nickel rich alloy, the ratio X^s_{Au}/X^s_{Ni} has been calculated by means of both eqs. (2) and (3). It can be seen that the results obtained by these two methods agree in most cases within 10% or so. For the gold-rich alloys we have used the calibration curve of fig. 6 which depends on the ratio $P_{Au\text{-}st}/P_{Ni\text{-}st}$ and is consequently related more closely to results obtained from eq. (3). In the following analysis, we therefore use the results for the nickel-rich alloy obtained by eq. (3), for maximum consistency.

4. Discussion

4.1. Theory

4.1.1. Energy effects

Most of the microscopic statistical treatments of interfacial segregation [2–9] in solid solutions assume a "two-phase" model, consisting of a bulk phase and an interface phase. For our purposes here, let us consider a crystal consisting of a two-component solid solution in which the first atom plane is taken to be the surface phase. By writing the total free energy of the crystal in a regular solution approxi-

mation (i.e. where the distribution of atoms is assumed to be random, but where the heat of mixing is assumed to be non-zero) and minimizing the free energy with respect to the compositions of both phases, it can be shown that [2,3,6]

$$(X_A^s/X_B^s) = (X_A^b/X_B^b)\exp(-\Delta H_a/kT), \tag{4}$$

where X_A^s and X_B^s are the atom fractions of component A and B in the surface phase, X_A^b and X_B^b are the corresponding quantities for the bulk phase, ΔH_a is the enthalpy or heat of adsorption of the segregating component and k and T are the Boltzmann constant and absolute temperature respectively.

The heat of adsorption, which is the driving force for the segregation process, represents the enthalpy change which results when an atom of the segregating species, located in the bulk, exchanges positions with an atom of the other species, located at the surface. This enthalpy change can be calculated, for example, on the basis of a nearest neighbor bond model, as was done originally by Defay et al. [2]. In that case, the energy of a crystal may be computed as a sum over all nearest neighbor bonds (these being assigned energies ϵ_{AA}, ϵ_{BB} and ϵ_{AB} depending on whether they lie between A–A, B–B or A–B pairs of atoms, respectively) with the result:

$$\Delta H_a = (\gamma_A - \gamma_B)\mathcal{A} + \omega\{Z_\ell(X_B^{s2} - X_A^{s2} + X_A^{b2} - X_B^{b2}) + Z_v(X_A^{b2} - X_B^{b2})\}, \tag{5}$$

where γ_A and γ_B are the surface energies of components A and B respectively, $\mathcal{A}$ is the surface area per atom, Z_ℓ is the number of lateral bonds made by an atom within its plane, Z_v is the number of bonds made by an atom to each adjacent plane of atoms (e.g. for an fcc crystal with a {111}-type surface, $Z_\ell = 6$ and $Z_v = 3$), and ω, the alloy parameter, is defined as

$$\omega \equiv \epsilon_{AB} - (\epsilon_{AA} + \epsilon_{BB})/2. \tag{6}$$

In the case of a regular solution, the alloy parameter can be related to the heat of mixing of the alloy [19]:

$$\omega = \Delta H_m/ZX_A^bX_B^b, \quad Z = \text{coordination number}. \tag{7}$$

Substituting this expression into eq. (5), and recognizing that $X_A + X_B = 1$ for both surface and bulk, it can be shown that:

$$\Delta H_a = (\gamma_A - \gamma_B)\mathcal{A} + (2\Delta H_m/ZX_A^bX_B^b)\{Z_\ell(X_A^b - X_A^s) + Z_v(X_A^b - \tfrac{1}{2})\}. \tag{8}$$

Eq. (8) is more useful than its bond model counterpart as all bond energies have been replaced by readily available thermodynamic properties of the system. However, it should be noted that this result was obtained without consideration of any size differences between the A- and B-atoms of the alloy.

In contrast to the method of Defay et al. [2], McLean [3] estimated the heat of adsorption for grain boundary segregation under the assumption that the driving force arises exclusively from size differences between the two types of atom present in a binary alloy. In general, the size (atomic radius) of a solute will differ from that

of the solvent, leading to a strain field around the solute atom, and an associated strain energy. McLean postulated that this strain energy would be eliminated by the exchange of a solute atom in the bulk with a solvent atom in the boundary. Here we make the analogous approximation that the solute strain energy is totally eliminated on exchange of a bulk solute atom with a surface solvent atom. While it is difficult to assess its validity, this approximation is probably more realistic for surface segregation than for grain boundary segregation since mechanical constraints at surfaces tend to be less severe than at internal interfaces. The expression for the elastic energy of a solute atom employed by McLean contains a quantity which is difficult to evaluate. Thus, we prefer to use an expression derived by Friedel [20] in which the elastic strain energy of a solute atom is written as:

$$E_{el} = 24\pi K G r_0 r_1 (r_1 - r_0)^2 / (3Kr_1 + 4Gr_0), \tag{9}$$

where K is the bulk modulus of the solute, G is the shear modulus of the solvent, r_0 is the radius of the solvent atom in the pure solvent and r_1 is the radius of the solute atom in the pure solute. This expression is valid within the approximation that the alloy behaves as a linear elastic continuum and in the limit of infinite dilution, since interaction between solute atoms is not accounted for. The heat of adsorption based solely upon this model would be simply:

$$\Delta H_a = -E_{el}. \tag{10}$$

As stated in the introduction, it is clear that the true heat of adsorption must include contributions from the physical effects leading to both eqs. (8) and (10). If we consider eq. (8), we see that the heat of adsorption depends, among others, on the heat of mixing. Now, if we employ an experimental value for the heat of mixing of the alloy, it will include any elastic strain energy contributions (as well as other non-ideal energy contributions) which may be present in the alloy. Thus, the form of eq. (8) (where ΔH_m multiplies both bulk and surface concentrations) will lead to the inclusion of solute strain energy contributions in the energies of both the surface and bulk phases. But we are contending here that the strain energy contribution to the surface phase is negligible. Thus, the simplest way of reflecting the absence of these solute strain energy effects in the surface phase is to set the total heat of adsorption equal to the sum of the right hand sides of eqs. (8) and (10), i.e.:

$$\Delta H_a = (\gamma_A - \gamma_B)\mathcal{A} + \frac{2\Delta H_m}{Z X_A^b X_B^b}\{Z_\ell (X_A^b - X_A^s) + Z_v (X_A^b - \tfrac{1}{2})\}$$

$$- \frac{24\pi K G r_0 r_1 (r_0 - r_1)^2}{3Kr_1 + 4Gr_0}. \tag{11}$$

Examination of eqs. (8) and (11) shows that both predict heats of adsorption which depend on surface composition. (Such "coverage dependent" heats of adsorption are quite common, for example, in the chemisorption of gases on metal sur-

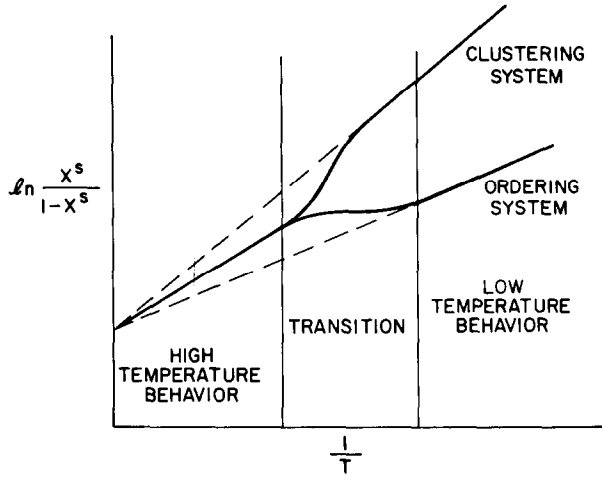

Fig. 7. Schematic of the trends predicted by eq. (4), with ΔH_a expressed according to either eq. (8) or eq. (11).

faces [21]). The consequences of this behavior are illustrated schematically in fig. 7, as a plot of $\ln[X^s/(1-X^s)]$ versus $1/T$ (which corresponds to the segregation law described by eq. (4)), for the case of an overall negative heat of adsorption. It is apparent that behavior is different in high and low temperature limits where X^s tends to X^b and to 1 respectively. In addition, the trends shown change with the sign of ΔH_m, which is positive for clustering systems, but negative for ordering systems. The above conclusions have been reached before, albeit in different form [6, 8]. However, it is worthwhile pointing out the behavior in the transition region. It can be seen that for clustering systems, the *apparent* heat of adsorption (i.e. one obtained from the slope of an experimental plot such as fig. 7) in the transition region, can be much larger than the actual heat of adsorption, which is bounded by the high and low temperature limiting values. Thus it is necessary to exercise extreme caution in the interpretation of experimental heats of adsorption extracted from the slopes of data plots of this type, and in comparisons between heats of adsorption obtained on different alloys in different temperature regimes.

According to eq. (4), we would expect any truly linear portion of a $\ln[X^s/(1-X^s)]$ versus $1/T$ plot to extrapolate to the bulk composition, but this is rarely observed [3]. This may be due partly to previous extrapolation of data that fell within the transition temperature region illustrated in fig. 7, since such a procedure would clearly lead to an extrapolated intercept (at $1/T = 0$), having a value quite different from the bulk composition. However, in addition to this difficulty, it is necessary to consider the possible modification of eq. (4) by entropy terms, which have been neglected thus far.

4.1.2. Entropy effects

The form of eq. (4) and specifically the appearance of an enthalpy term rather than a free energy term in the argument of the exponential, is a direct consequence of the use of a regular solution approximation, where the only entropy contribution accounted for is that assumed to arise from a random distribution of atoms in the solid solution. Thus, eq. (4) is more completely stated as follows:

$$\frac{X_A^s}{X_B^s} = \frac{X_A^b}{X_B^b} \exp\left(\frac{-\Delta F_a}{kT}\right) = \frac{X_A^b}{X_B^b} \exp\left(\frac{\Delta S_a}{k}\right) \exp\left(\frac{-\Delta H_a}{kT}\right), \tag{12}$$

where ΔF_a and ΔS_a are the free energy and entropy of adsorption respectively.

The terms which must enter an expression for ΔS_a can be determined from eq. (11) by inspection, since the entropy contributions must parallel the enthalpy contributions in that equation. The surface energy terms, γ, in eq. (11) possess a temperature dependence and are, strictly speaking, surface free energies. Thus, an expression for ΔS_a should include corresponding specific surface entropy terms. The quantity ΔH_m was introduced by the use of eq. (7), which is valid only in the limit of a regular solution. In a real solid solution, we must include a contribution from the excess entropy of mixing, ΔS_m^E. This latter quantity is zero, by definition, in a regular solution and represents all entropy contributions over and above those resulting from random mixing [19]. Finally, the elastic energy term, eq. (9) has generally been considered to represent an elastic free energy, having a temperature dependence which arises primarily from the temperature dependence of the elastic moduli, K and G. Thus, to the same degree of approximation as eq. (11), we may represent the entropy of adsorption as:

$$\Delta S_a = (S_A - S_B)\mathcal{A} + \frac{2\Delta S_m^E}{ZX_A^b X_B^b}\{Z_\varrho(X_A^b - X_A^s) + Z_v(X_A^b - \tfrac{1}{2})\}$$

$$+ \frac{d}{dT}\left\{\frac{24\pi KGr_0 r_1 (r_0 - r_1)^2}{3Kr_1 + 4Gr_0}\right\}, \tag{13}$$

where S_A and S_B are the specific surface entropies of the pure components.

4.2. Comparison of present experiments with theory

The data of table 2 are plotted in figs. 8 and 9. The lines shown are calculated from the theory, using the following physical constants. Surface energies for pure nickel and gold of 1850 and 1400 erg/cm^2 respectively were obtained from compilations published by Overbury et al. [17] and Winterbottom [22]. The surface area per atom was considered to be equal to that of pure nickel for nickel-rich alloys and equal to that of gold for gold rich alloys. It was assumed that the atomic packing in a {100} type face constituted a reasonable average value for the poly-

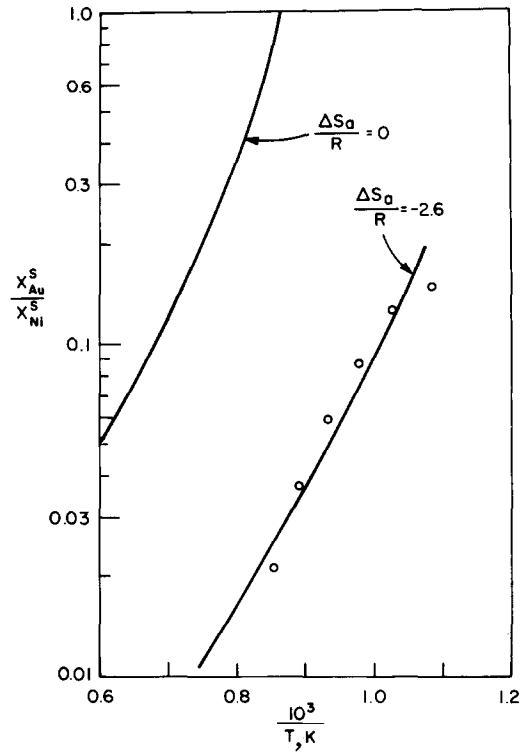

Fig. 8. Comparison of the data for the Ni–0.05 at% Au alloy with theoretical curves calculated both with and without an entropy of adsorption contribution.

crystalline materials used in this investigation; thus, $\mathcal{A}$ was calculated from

$$\mathcal{A} = a_0^2/2 ,$$

where a_0 is the lattice parameter of the pure metal ($a_0 = 3.524$ Å and 4.078 Å respectively for nickel and gold). Values of $\Delta H_m/(X_A^b X_B^b)$ of 7144 cal/g-atom and 5555 cal/g-atom for nickel- and gold-rich alloys respectively were obtained from Hultgren et al. [23]. The elastic moduli were taken from Gschneidner [24]: $K = 1.90 \times 10^6$ and 1.766×10^6 kg/cm^2, and $G = 0.765 \times 10^6$ and 0.281 kg/cm^2 for nickel and gold respectively. Finally the various radii, r, were computed from the relation:

$$r = \sqrt{2}a_0/4 .$$

Neglecting entropy effects for the time being (i.e. assuming $\Delta S_a = 0$ in eq. (12)), the above data allow computation of the following segregation laws:

$$X^s_{Au}/X^s_{Ni} = 5.0 \times 10^{-4} \exp\{(6397 + 4763 X^s_{Au} + 8665)/RT\} . \quad (14a)$$

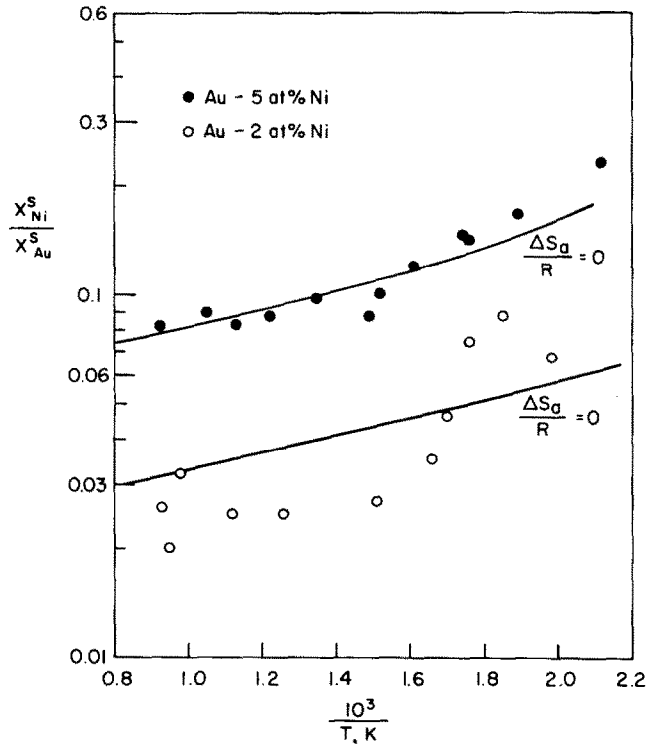

Fig. 9. Comparison of the data for two gold-rich alloys with theoretical curves calculated without an entropy of adsorption contribution.

for the Ni – 0.05 at% Au alloy,

$$X^s_{Ni}/X^s_{Au} = 5.26 \times 10^{-2} \exp\{(-3903 + 3703X^s_{Ni} + 4496)/RT\} \quad (14b)$$

for the Au – 5 at% Ni alloy, and

$$X^s_{Ni}/X^s_{Au} = 2.04 \times 10^{-2} \exp\{(-3680 + 3703X^s_{Ni} + 4496)/RT\} \quad (14c)$$

for the Au–2 at% Ni alloy, where R is the gas constant in cal/g-atom · K. The third term in the exponential represents the solute strain energy contribution, and is comparable in magnitude to the surface energy and alloy parameter contributions.

If we take $X^s \approx 0.1$, it can be seen right away that a large negative heat of adsorption is obtained for the nickel-rich alloy, predicting strong segregation of gold. This result is obtained because all of the effects included in the theory tend to reinforce each other. The surface energy of gold is lower than that of nickel, this effect will therefore drive gold to the surface; the heat of mixing tends to favor segregation of

the solute (gold in this case) in dilute clustering alloys; and finally, the solute strain energy term always tends to favor segregation of the solute.

In the case of gold rich alloys, and for a value of $X^s \approx 0.1$, eqs. (14b) and (14c) yield only a small, negative heat of adsorption, predicting weak surface segregation of nickel. This results because the effects included in the model now tend to offset each other. The surface energy effect still favors the segregation of gold to the surface, but the alloy parameter and solute strain energy terms tend to favor segregation of the solute (nickel in this case) and are large enough to lead to a net segregation of nickel. Both predictions are in good agreement with the behavior observed in these alloys.

The curves corresponding to eqs. (14) and plotted in figs. 8 and 9, and are labelled $\Delta S_a/R = 0$. The calculated curve shown in fig. 8, for the case of the nickel-rich alloy, lies about one order of magnitude above the data, indicating poor quantitative agreement between theory and experiment. On the other hand, the agreement between the calculated curve and the data from the Au–5 at% alloy, shown in fig. 9, is very good. Comparison of theory and experiment for the case of the Au–2 at% Ni is reasonable, although less meaningful in view of the excessive experimental scatter in that case (stemming from the relatively low nickel surface concentrations in that alloy).

Thus far, the entropy effects mentioned in section 4.1.2 have been neglected. If these are invoked, then good agreement between theory and experiment can be obtained by *assuming* an entropy contribution of -2.6 eu (entropy units), i.e. by multiplying the right hand side of eq. (14a) by $\exp(-2.6)$. The calculated curve obtained this way is also shown in fig. 8 and matches the data quite closely. However, one important question remains to be answered: Why is it necessary to invoke entropy effects in order to match theory with experiment in the case of nickel-rich alloys, when no entropy effects are needed for reasonable theoretical predictions in the case of gold–nickel alloys?

We shall attempt to answer this question by estimating the entropy contribution for both types of alloy, by means of eq. (13), bearing in mind that these estimates are necessarily crude. In examining eq. (13), we see that an estimate of the entropy factor requires values of the specific surface entropies of gold and nickel, the excess entropies of mixing and the elastic solute entropy. We take these up in that order.

The specific surface entropy of solid metals is difficult to measure and the values quoted in the literature are generally uncertain [25]. In contrast, the specific surface entropy of liquid metals is somewhat better characterized and it is generally expected that some reduction in surface entropy will result on melting. Jones and Leak [25] have summarized the available surface entropy data for several metals, among them nickel and gold, in both the liquid and solid states. For nickel, they quote values of 1.1 and 0.98 erg/cm^2 K in the solid and liquid states respectively, while for gold they report values of 0.5 and 3.2 in the solid state and 0.1 and 0.5 erg/cm^2 K in the liquid state. Thus, it is not unreasonable to pick 1 erg/cm^2 K for nickel and 0.5 erg/cm^2 K for gold as an approximately self consistent set of values

for these metals in the solid state. These values translate into $S\mathcal{A} = 3.01$ eu and 4.49 eu for gold and nickel respectively.

The excess entropies of mixing for the gold–nickel system have been given by Hultgren et al. [23], and these yield $\Delta S_m^E/(RX_A^s X_B^s)$ values of 0.90 and 0.78 eu for nickel-rich and gold-rich alloys respectively.

Finally, the elastic solute entropy can be obtained from the third term on the right hand side of eq. (13), by using data for the temperature dependence of the appropriate elastic moduli, listed by Simmons and Wang [26]. For metals, the fractional temperature change of elastic moduli, e.g. $(1/K)(dK/dT)$, tends to be greater than thermal expansion coefficients, $(1/r)(dr/dT)$, by at least an order of magnitude; thus, thermal expansion effects have been neglected here. This procedure leads to values of 1.13 and 0.65 eu for nickel and gold-rich alloys respectively.

Combining the above results, we obtain:

$$\Delta S_a/R = -1.78 - 0.6X_{Au}^s - 1.13 \tag{15a}$$

for the Ni – 0.05 at% Au alloy,

$$\Delta S_a/R = 1.27 - 0.52X_{Ni}^s - 0.65 \tag{15b}$$

for the Au – 5 at% Ni alloy, and

$$\Delta S_a/R = 1.24 - 0.52X_{Ni}^s - 0.65 \tag{15c}$$

for the Au – 2at% Ni alloy.

Taking $X^s \approx 0.1$, we obtain a total value $\Delta S_a/R$ of about -3.0 eu for the nickel-rich alloy and about 0.55 eu for the gold-rich alloys. These results follow the general trends displayed by the calculated heats of adsorption; i.e., the different model contributions to the entropy tend to reinforce each other in the case of nickel-rich alloys, leading to a large negative entropy of adsorption, but tend to offset each other in the case of gold-rich alloys yielding a small positive entropy of adsorption. These estimates, therefore, provide a reasonable framework for understanding the empirical results, $\Delta S_a/R = -2.6$ and 0, obtained by fitting the data for nickel- and gold-rich alloys respectively. A more quantitative comparison of the calculated and empirical entropy effects is unwarranted in view of the uncertainties in the surface entropy data.

4.3. Comparison of other experiments with theory

Two other studies of surface segregation in nickel–gold alloys have been published: a rather cursory study of three different nickel-rich alloys, all equilibrated at 1300 K, by Williams and Boudart [10], and a more detailed study of segregation on the (111) surface of nickel-rich alloy single crystals by Burton et al. [11]. We now proceed to a comparison of those results with the present model.

Fig. 10 shows the points obtained by Williams and Boudart together with a

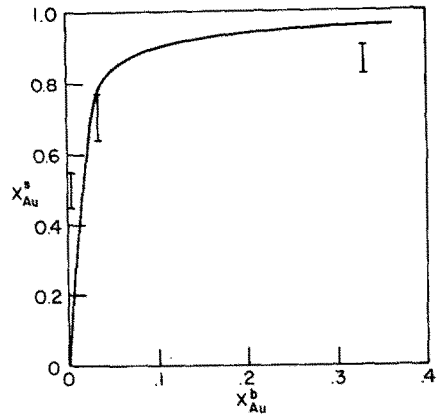

Fig. 10. Comparison of the data of Williams and Boudart [10] with theory.

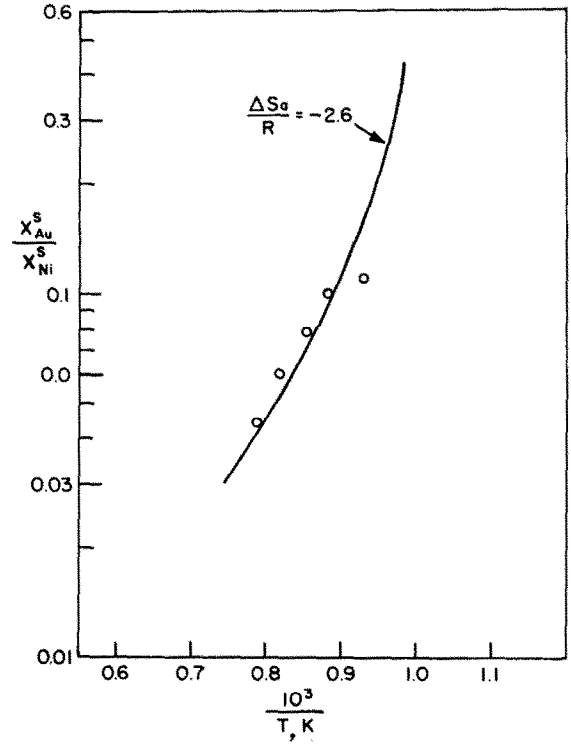

Fig. 11. Comparison of the data of Burton et al. [11] with theory.

theoretical curve using the parameters employed in section 4.2, including the entropy contribution of −2.6 eu. As can be seen, the agreement is reasonable, with discrepancies believed to stem from the use of the Auger Ni 840 eV transition for the determination of surface nickel concentration (a procedure likely to overstimate the nickel content of the surface because that transition is far less surface sensitive than the Ni 61 eV transition) as well as our extension of the theory to non-dilute alloys.

The theory is compared in fig. 11 with the data obtained for a Ni–0.2 at% Au alloy by Burton et al. [11]. The curve has been computed for a {111}-type surface, by adjusting Z_ϱ and Z_v of eq. (11) and using the relation:

$$\mathcal{A}_{(111)} = \sqrt{3}a_0^2/4 .$$

Otherwise, the parameters used were the same as those employed to compute the curve labelled $\Delta S_a/R = -2.6$ in fig. 8. It can be seen that the agreement between the theory and these results is excellent.

These comparisons provide further evidence of the conceptual validity of the present model.

5. Closing comments

It would be too time consuming and repetitive to trace back all of the approximations and assumptions which have led to the computation of the heats of adsorption, and to the transformation of the raw experimental results into surface compositions. However, in view of the above simplifications, it is surprising that such good agreement between experiment and theory has been obtained. On the other hand, the differences in experimental segregation behavior between gold-rich and nickel-rich alloys are quite significant, and in view of the good agreement with theory, one must conclude that the present theoretical description accounts correctly for all major effects. In addition to prediction of the heats of adsorption, the present formalism also provides estimates of entropy effects, which have been shown to be a useful adjunct in rationalizing differences between the relationship of surface to bulk composition in alloys from opposite ends of a given phase diagram. Thus, the importance of *both* surface energy and solute strain energy effects in surface segregation phenomena has been established, and the simple combination of these effects into a single formalism (e.g. eqs. (11) and (13)) has been generally justified by the results.

Acknowledgement

The authors wish to thank Drs. D.W. Hoffman, W.C. Johnson and W.L. Winterbottom for useful discussions and a critical review of the manuscript.

References

[1] J.W. Gibbs, The Scientific Papers of J. Willard Gibbs, Vol. 1 (Dover, New York, 1961) p. 219.
[2] R. Defay, I. Prigogine, A. Bellemans and D.H. Everett, Surface Tension and Adsorption (Wiley, New York, 1966) p. 158.
[3] D. McLean, Grain Boundaries in Metals (Oxford Univ. Press, London, 1957).
[4] J.L. Meijering, Acta Met. 14 (1966) 251.
[5] R.A. VanSanten and W.M.H. Sachtler, J. Catalysis 33 (1974) 202.
[6] F.L. Williams and D. Nason, Surface Sci. 45 (1974) 377.
[7] K. Binder, D. Stauffer and V. Wildpaner, Acta Met. 23 (1975) 1191.
[8] V.S. Sundaram and P. Wynblatt, Surface Sci. 52 (1975) 569.
[9] J.J. Burton, E. Hyman and D. Fedak, J. Catalysis 37 (1975) 106.
[10] F.L. Williams and H. Boudart, J. Catalysis 33 (1973) 438.
[11] J.J. Burton, C.R. Helms and R.S. Polizzotti, J. Vacuum Sci. Technol. 13 (1976) 204.
[12] P.W. Palmberg and T. Rhodin, J. Appl. Phys. 39 (1968) 2425.
[13] J.W. Ridgeway and D. Haneman, Surface Sci. 26 (1971) 683.
[14] Handbook of Auger Electron Spectroscopy (Physcial Electronics Industries, Edina, Minn. 1972).
[15] H.J. Mathieu and D. Landolt, Surface Sci. 53 (1975) 228.
[16] P. Braun and W. Farber, Surface Sci. 47 (1975) 57.
[17] S.H. Overbury, P.A. Bertrand and G.A. Somorjai, Chem. Rev. 75 (1975) 547.
[18] G.A. Somorjai and S.H. Overbury, Faraday Discussions of the Chemical Society, No. 60 (1975) 279.
[19] R.A. Swalin, Thermodynamics of Solids (Wiley, New York, 1972).
[20] J. Friedel, Advan. Phys. 3 (1954) 446.
[21] D.O. Hayward and B.M.W. Trapnell, Chemisorption (Butterworths, London, 1964) p. 194.
[22] W.L. Winterbottom, Structure and Properties of Surfaces (Maruzen, Tokyo, 1973) p. 35.
[23] R. Hultgren, P.A. Desai, D.T. Hawkins, M. Gleiser and K.K. Kelly, Selected Values of the Thermodynamic Properties of Binary Alloys (Am. Soc. for Metals, Metals Park, 1973).
[24] K.A. Gschneidner, in: Solid State Physics, Vol. 16, Eds. F. Seitz and D. Turnbull (Academic Press New York, 1964) p. 275.
[25] H. Jones and G.M. Leak, Met. Sci. J. 1 (1967) 211.
[26] G. Simmons and H. Wang, Single Crystal Elastic Constants and Calculated Aggregate Properties (MIT Press, Cambridge, 1971).